J Nanopart Res (2025) 27:218
https://doi.org/10.1007/s11051-025-06420-0

RESEARCH

Synthesis and characterization of ultrasmall rhenium nanoparticles (1.5 nm)

Niklas Kost · Oleg Prymak · Kateryna Loza · Marc Heggen · Cristiano L. P. Oliveira · Christine Beuck · Peter Bayer · Matthias Epple

Received: 30 April 2025 / Accepted: 4 August 2025 / Published online: 13 August 2025

Abstract Ultrasmall rhenium nanoparticles were prepared by a reduction of rhenium trichloride with sodium borohydride in water capped with the tripeptide glutathione. The particles were approximately spherical with an average diameter of 1.5 nm and had a high degree of internal crystallinity as shown by transmission electron microscopy and X-ray powder diffraction. They were well dispersible in water as differential centrifugal sedimentation (DCS), ^{1}H-NMR DOSY spectroscopy (nuclear magnetic resonance–diffusion-enhanced spectroscopy), and small-angle X-ray scattering (SAXS) showed. ^{1}H-NMR spectroscopy and ^{13}C-NMR spectroscopy confirmed that glutathione was attached to the nanoparticle via the terminal thiol group of cysteine. Upon heating in oxygen, the nanoparticles were converted into dirhenium heptoxide which evaporated above 360 °C.

Keywords Nanoparticles · Rhenium · Ultrasmall · Glutathione

Supplementary Information The online version contains supplementary material available at https://doi.org/10.1007/s11051-025-06420-0.

N. Kost · O. Prymak · K. Loza · M. Epple (✉)
Inorganic Chemistry and Centre of Nanointegration Duisburg-Essen (CENIDE), University of Duisburg-Essen, Universitaetsstr, 5-7, Essen 45117, Germany
e-mail: matthias.epple@uni-due.de

M. Heggen
Ernst Ruska Centre for Microscopy and Spectroscopy with Electrons, Forschungszentrum Jülich, Jülich 52428, Germany

C. L. P. Oliveira
Institute of Physics, University of São Paulo, São Paulo 05508-090, Brazil

C. Beuck · P. Bayer
Structural & Medicinal Biochemistry, University of Duisburg-Essen, Universitaetsstr. 2-5, Essen 45117, Germany

Introduction

Metal nanoparticles are of interest due to their different properties compared to the corresponding bulk material. Their small size and large specific surface area lead to distinct physicochemical properties that make them interesting for applications in catalysis [1–3], imaging [4], and electrochemistry [5]. A major application of rhenium nanoparticles is the reforming of petroleum [6] and biomass [7, 8]. This reaction benefits from the high catalytic efficiency of bimetallic rhenium-platinum nanoparticles [9]. In addition, rhenium nanoparticles catalyze the isomerization of alkenols [10]. Alloyed rhenium nanoparticles were also tested in the oxygen reduction reaction (ORR) for fuel cells and in electrocatalysis [11]. More recently, rhenium nanoparticles have been discussed as supported catalysts in the hydrogen evolution reaction (HER) in electrochemical water splitting [12]. Ramirez et al. gave a comprehensive overview

on the application of rhenium-based catalysts in that area [13]. Rhenium nanoparticles have also been studied as catalysts for the thermal decomposition of ammonium perchlorate, a solid propellant [14], and as catalysts for the reduction of 4-nitrophenol to 4-aminophenol [15, 16]. In a biomedical application, ^{188}Re isotope nanoparticles (< 50 nm) were proposed for radiotherapy of spleen, bone marrow, and other tumors as they are high-energy beta radiation emitters [17, 18].

Many syntheses were reported for nanoparticles of silver, gold, and platinum metals [19–21]. In contrast, there are only a few reported syntheses of uniform water-dispersible rhenium nanoparticles. In general, rhenium nanoparticles can be synthesized by different methods. One option is the reduction of rhenium salts by metallic sodium in liquid ammonia [22, 23]. Another possibility is the pulsed-laser decomposition of ammonium perrhenate(+ VII), NH_4ReO_4, or of dirhenium decacarbonyl, $Re_2(CO)_{10}$, that leads to rhenium nanoparticles of 20 to 60 nm in diameter [10]. The reduction of potassium hexachloridorhenate(+ IV), K_2ReCl_6, with hydrazine resulted in unstable nanoparticle dispersions that dissolved in water by oxidation to perrhenate ions [24]. The thermal decomposition of ammonium perrhenate and dirhenium decacarbonyl led to a mixture of rhenium nanoparticles with various rhenium oxides [25]. Shiri et al. have reviewed the microemulsion-based synthesis to prepare metal nanoparticles of osmium, rhenium, iridium, and rhodium and reviewed the state-of-the-art of this synthesis pathway [26]. However, all these syntheses either led to polydisperse nanoparticles, non-water-dispersible nanoparticles, or poor yields. The rhenium nanoparticles also tend to oxidize within days in contact with air or water, usually demonstrated by X-ray photoelectron spectroscopy (XPS) [14, 16, 24, 27]. Babu and Mucalo prepared agglomerated rhenium nanoparticles in the size range of several hundred nanometers without a capping agent that contained rhenium in a variety of oxidation states between + II and + VII as shown by XPS. This was ascribed to oxidation in the dispersant water that also contained dissolved oxygen [27]. It has been shown that rhenium nanoparticles undergo surface oxidation within days in contact with air and water [24].

Water-dispersible smaller nanoparticles with a diameter of 3 nm ("ultrasmall nanoparticles") [28–31] are particularly promising due to their high specific surface area. Here, we report a facile and robust synthesis of uniform ultrasmall rhenium nanoparticles, based on the reduction of rhenium trichloride with sodium borohydride, colloidally stabilized by the tripeptide glutathione.

Materials and methods

Chemicals

We used rhenium(III) chloride (99.99%, AlfaAesar), glutathione (98%, Sigma-Aldrich), sodium borohydride (98%, Sigma-Aldrich), methanol (HPLC grade, Fisher Scientific), deuterium oxide (99.9%, Deutero), and Amicon Ultra Spin filters (3 kDa, Merck). For differential centrifugal sedimentation (DCS), a PVC nanoparticle calibration standard (Lot#123, 263 nm, CPS Instruments Inc.) and dodecane (99%, ABCR) were used.

Ultrapure water (Purelab Ultra instrument, 18.2 MΩ, ELGA) was used for all experiments. All glassware was cleaned by boiling once with concentrated nitric acid (65% in water, Fisher Scientific) and then washed with water.

Synthesis of glutathione-stabilized rhenium nanoparticles

A synthesis of gold nanoparticles reported by Schaaff et al. was adapted for rhenium [32, 33]. Briefly, rhenium trichloride ($ReCl_3$, 20 mg, 68 µmol, 1 eq.) was dissolved in 50 mL methanol in a 100-mL round-bottom flask. Glutathione (GSH, 42 mg, 136 µmol, 2 eq.) dissolved in 20-mL ice-cold water was quickly added. The solution changed its color from light-reddish to slightly violet within 10 min, indicating the formation of rhenium-glutathione complexes. $NaBH_4$ (51.7 mg, 1.36 mmol, 20 eq.) dissolved in 5-mL ice-cold water was rapidly added, leading to a color change of the dispersion to black-brown, indicating nanoparticle formation. Methanol was removed with a rotary evaporator in vacuum. The black nanoparticle dispersion was transferred to 3-kDa spin filters. The nanoparticles were isolated by spin filtration for 45 min at 4000 rpm (2500 g) and washed four times with water under the same conditions. The yield was 5.1 mg, based on rhenium (27.4 µmol, 40%) by ICP-MS. The dispersed nanoparticles were characterized by ^{1}H-NMR

spectroscopy (600 MHz, D_2O), $\delta = 3.84–3.72$ (m, 3H), 3.33–3.26 (m, 1H), 3.05–2.93 (m, 1H), 2.58–2.53 (m, 2 H), and 2.19–2.12 (m, 2H) ppm, and ^{13}C-NMR spectroscopy (151 MHz, D_2O), $\delta = 175.1$, 171.9, 54.2, 52.7, 43.6, 38.8, 31.4, and 26.2 ppm.

Inductive coupled plasma mass spectrometry (ICP-MS)

The rhenium concentration in the product was determined on freeze-dried nanoparticles after microwave digestion (MARS 6; CEM) by inductively coupled plasma mass spectrometry (Spectro Arcos instrument; Kolbe Microanalysis Laboratory, Fraunhofer Institute Umsicht, Oberhausen). The error of the analysis was 0.015%.

Transmission electron microscopy

Transmission electron microscopy was performed with a FEI TEM 80–300 microscope [34]. The sample was imaged at an accelerating voltage of 300 kV. The nanoparticle dispersion was applied to a copper grid coated with an ultrathin amorphous carbon film and subsequently dried in air at ambient temperature. The size of the nanoparticles was measured with the program ImageJ [35].

X-ray powder diffraction (XRD)

X-ray powder diffraction was performed with a Bruker D8 Advance powder diffractometer in Bragg–Brentano reflection mode with Cu Kα radiation ($\lambda = 1.5418$ Å; 40 kV, 40 mA). The water-dispersed nanoparticles were drop-cast on a silicon single crystal sample holder in order to minimize scattering and gently dried with warm air. Each sample was measured from 20° to 90° 2θ with a step size of 0.02° and a counting time of 8 s, resulting in a total measurement time of 8.4 h. Qualitative phase analysis was performed with the program Diffrac.Suite EVA V7.1 (Bruker) with the pattern of Re (#00–005-0702) from the ICDD database. After instrumental calibration with the reference material LaB_6 from NIST (SRM 660b), quantitative Rietveld refinement was performed with the software TOPAS 7.0 (Bruker) to calculate the lattice parameters and the average crystallite size from diffraction peak broadening.

Small-angle X-ray scattering (SAXS)

SAXS measurements were performed on a laboratory base system Xenocs-Xeuss 2.0 (EMUSAXS center at the Institute of Physics, University of São Paulo). This system uses a microfocus source Genix3D (Cu Kα radiation), Fox3D focusing mirrors, and two sets of scatterless slits. The 2D scattering intensities were collected on a Dectris-Pilatus 300k detector. The obtained scattering images were integrated with the program package Fit2D [36], leading to 1D curves of the scattering intensity as a function of the momentum transfer modulus q, defined as $q = 4\pi\sin\Theta/\lambda$. The liquid samples were placed on custom-made reusable sample holders, consisting of borosilicate glass capillaries (1.5 mm of diameter) glued on stainless steel cases and closed with rubber caps. Therefore, the sample holders could be cleaned by washing, allowing the measurements of samples and buffers in the same capillaries, thereby optimizing the data quality. Pure water (20 °C) was used for normalization to an absolute scale. The estimation of uncertainties and the data treatment were performed with the program SuperSAXS [37].

For the modeling of the scattering intensity, a model of polydisperse spheres with radius R and polydispersity σ was used. The intensity is given by

$$I(q) = S_C \cdot P(q, R, \sigma) + Back \quad (1)$$

where P is the form factor of polydisperse spheres, S_C is a scale factor, and *Back* is a constant background. All mathematical details of the modeling procedure can be found in Ref. [38].

NMR spectroscopy

The freeze-dried nanoparticles were redispersed in 500 µL D_2O by treatment for 2 h in an ultrasonic bath. The dispersion was filled into a 5-mm NMR tube and measured on a Bruker Avance III 600 MHz spectrometer at 25 °C.

DOSY NMR spectroscopy

DOSY-^{1}H-NMR spectroscopy of glutathione-coated nanoparticles dispersed in 90% H_2O/10% D_2O was performed with a Bruker Avance III 700 MHz

spectrometer with a 5-mm TCI cryoprobe with a *z*-gradient at 25 °C. A ^{1}H-DOSY pulse sequence from Bruker was equipped with presaturation for water suppression. The spectra were measured with a diffusion time of $\Delta = 100$ ms and a pulsed gradient duration of $\delta = 3.5$ ms. The gradient strength was incremented from 5 to 95% of the maximum gradient strength (66 G cm^{-1} for a smoothed square gradient pulse) in 32 linear steps. The spectra were processed with the program Topspin 3.5 (Bruker). The linearized diffusion data were plotted and fitted according to the Stejskal-Tanner Eq. [39, 40]:

$$In\left(\frac{I}{I_0}\right) = -\gamma^2\,\delta^2\left(\triangle - \frac{\delta}{3}\right)\cdot D\cdot G^2 \tag{2}$$

with I the signal intensity, I_0 the signal intensity without gradient, γ the gyromagnetic ratio of ^{1}H, δ the diffusion gradient pulse length, Δ the diffusion delay, G the gradient strength, and D the translational diffusion coefficient.

The linearized relative intensities of all ^{1}H signals were averaged. Error bars represent the standard deviation of these signals. While the standard error of the Stejskal-Tanner fit itself is small (< 2%), we estimate the error of the diffusion coefficient to ± 20% due to manual integration and potentially overlaying small signals from impurities.

The hydrodynamic diameter was calculated according to the Stokes–Einstein Eq. [41]:

$$d_H = \frac{k_B\cdot T}{3\pi\cdot\eta\cdot D} \tag{3}$$

with d_H the hydrodynamic diameter, k_B the Boltzmann constant, T the temperature in K, η the dynamic viscosity at 25 °C, and D the translational diffusion coefficient.

Differential centrifugal sedimentation (DCS)

Differential centrifugal sedimentation was carried out with a CPS Instruments DC 24000 disc centrifuge, operating at 24,000 rpm and 29,000 relative centrifugal force (29,000 × g). A density gradient was obtained by overlaying with two sucrose solutions with concentrations of 8 and 24 wt%, respectively. Dodecane (0.5 mL) was added to the top layer to prevent evaporation. Prior to each measurement, a dispersion of poly(vinyl chloride) (PVC) with a defined hydrodynamic diameter of 263 nm dispersed in water was measured for calibration. The volume of the added nanoparticle dispersion was 100 µL in water. The hydrodynamic diameter of the nanoparticles was calculated with the density of elemental rhenium (21.03 g cm^{-3}).

UV–Vis spectroscopy

UV–Vis spectroscopy was performed with quartz glass cuvettes from 200 to 800 nm (600 µL) in a Genesis 50 instrument (ThermoScientific). The background of pure water was subtracted.

Thermogravimetry

Thermogravimetry was carried out with a Netzsch STA 449 F3 thermobalance. Fifteen to 20 mg of the sample were heated in an open aluminum crucible with a rate of 5 K min^{-1} from 25 to 1000 °C in a dynamic oxygen atmosphere. In addition, sample aliquots were heated to 300, 500, and 700 °C in the thermobalance under the same conditions, freely cooled to room temperature, and examined by X-ray powder diffraction.

Results and discussion

Ultrasmall rhenium nanoparticles were synthesized by reduction in water and stabilized with glutathione. Glutathione is attached to the rhenium nanoparticle surface, probably via the thiolate group of cysteine [18], and protects the nanoparticles from growth and agglomeration [42]. UV–Vis spectroscopy showed that no larger (plasmonic) nanoparticles were present (Fig. 1). The UV–Vis spectrum showed a strong absorption below 250 nm due to the ligand glutathione [43]. In addition, a small shoulder was observed around 370 nm, possibly due to small rhenium clusters or the presence of oxidized rhenium species [18, 24]. Creighton and Eadon have discussed the UV spectra of colloidally dispersed metal nanoparticles in a very comprehensive contribution, covering 52 metallic elements. They calculated UV spectra for 10-nm particles in vacuum and in water, based on the Mie scattering theory. For rhenium, they predicted a moderate increase in absorption below 400

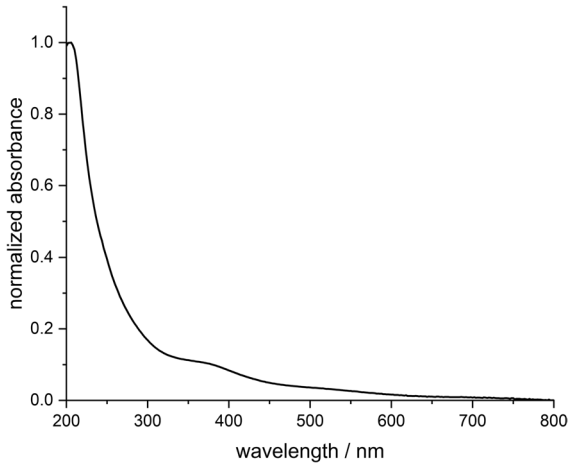

Fig. 1 UV–Vis spectrum of glutathione-coated ultrasmall rhenium nanoparticles, dispersed in water

nm that became steeper below 300 nm, in good agreement with our results [44].

The metal core diameter was determined by high-resolution transmission electron microscopy (HRTEM; Fig. 2). The *d*-spacing of the FFTs matched the rhenium hcp phase. The average particle diameter was 1.7 ± 0.5 nm with a monomodal particle size distribution. Figure 3 shows infrared spectra which demonstrate the presence of the capping agent glutathione on the nanoparticles.

Small-angle X-ray scattering (SAXS) results of water-dispersed nanoparticles are shown in Fig. 4. From the modeling, we obtained an average core diameter of 1.2 ± 0.2 nm, indicating well-dispersed spherical nanoparticles.

A complementary method to determine the hydrodynamic diameter is differential centrifugal sedimentation (DCS). The average particle size by DCS was 1.5 ± 0.3 nm (Fig. 5). Note that ultrasmall particles appear systematically smaller in DCS because their effective density is lower than that of the metallic core due to the surrounding ligand shell [45].

The ligand on the particle surface can be analyzed by solution NMR spectroscopy. For ultrasmall metal nanoparticles, such spectra can be analyzed but are usually accompanied by strongly broadened NMR peaks [46–49]. While NMR studies on nanoparticles of gold [50, 51], silver [52–54], and palladium [54, 55] have already been reported, there are no NMR studies on dispersed ultrasmall rhenium nanoparticles so far.

The ^{1}H-NMR spectrum (Fig. 6) did not show sharp signals; i.e., there was no residual dissolved glutathione in solution. The five broad signals in the spectrum can be assigned to glutathione bound

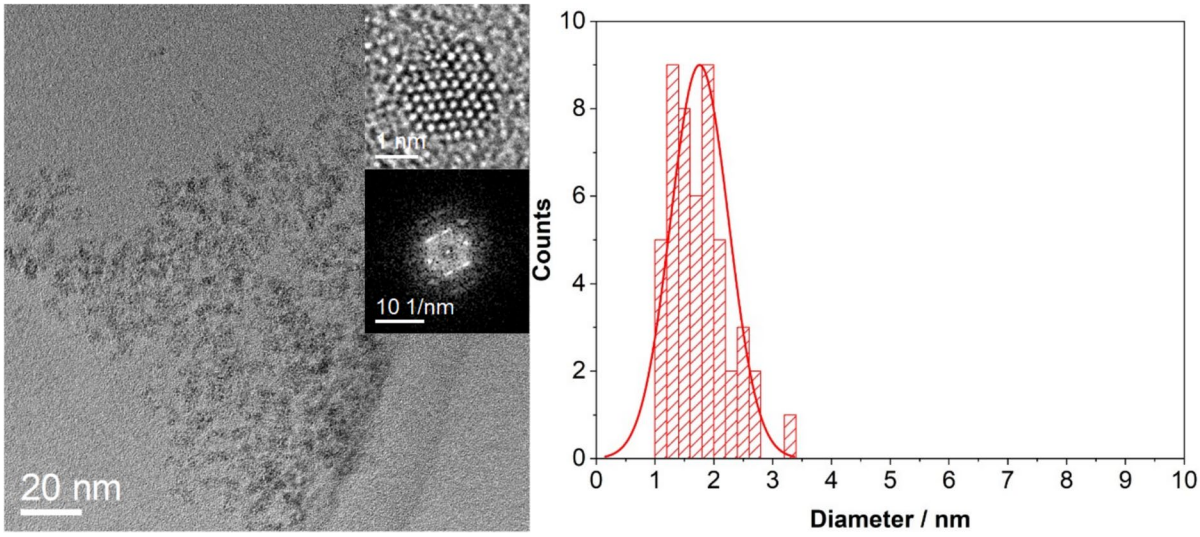

Fig. 2 Left: HRTEM image of glutathione-coated ultrasmall rhenium nanoparticles, with insets displaying the magnified view of a single particle and its corresponding FFT pattern. Right: The particle size distribution as determined from 50 individual nanoparticles

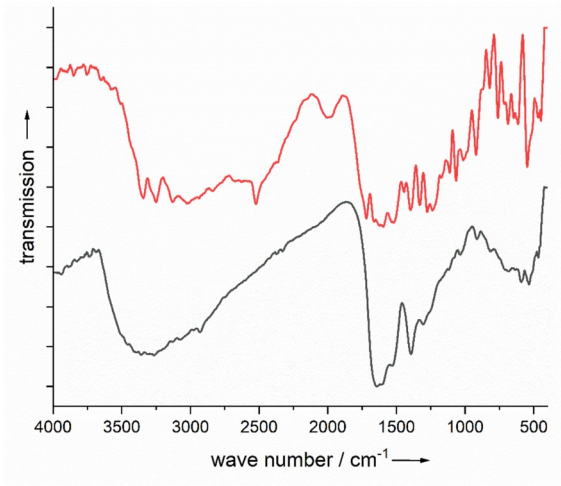

Fig. 3 Infrared spectra of glutathione (top) and glutathione-capped ultrasmall rhenium nanoparticles (bottom). They demonstrate the presence of glutathione on the nanoparticle surface where it acts as a stabilizing agent

to the nanoparticle surface via sulfur in agreement with earlier results on glutathione-capped ultrasmall gold nanoparticles [53]. This is supported by ^{1}H-^{1}H-COSY, ^{13}C, and ^{1}H-^{13}C-HSQC NMR spectra (see Supporting Information, Figures S1 to S3). We can conclude that the intact glutathione ligand is present on the nanoparticle surface. The fact that there are no sharp NMR signals underscores that glutathione is firmly attached to the rhenium particle surface and not in a dynamic adsorption/desorption equilibrium.

^{1}H-diffusion order spectroscopy (^{1}H-DOSY) gave the hydrodynamic diameter of the water-dispersed nanoparticles [39]. Figure 7 shows the Stejskal-Tanner plot of the ^{1}H-DOSY experiment. The nanoparticles in the sample diffused more slowly ($D = 1.82\ 10^{10}$ m^2 s^{-1}) than the dissolved (free) ligands, which means that the ligand was firmly bound to the surface. This corresponds to a hydrodynamic diameter of the dispersed nanoparticles of 2.2 ± 0.4 nm. The difference to the core diameter by SAXS (1.2 nm) and HRTEM (1.7 nm) indicates that the hydrated ligand shell has a thickness of about 0.3 to 0.5 nm, in agreement with earlier results of peptides attached to ultrasmall gold nanoparticles [56]. In the nanoparticle dispersion, no dissolved glutathione with high diffusion coefficient was observed by DOSY, confirming the absence of unbound glutathione.

It shall be emphasized here that NMR spectroscopy provides invaluable data on the nanoparticle, which are almost impossible to obtain by other methods. Although the NMR peaks are broadened and shifted with respect to the dissolved ligands, they give information on the presence and integrity of the ligands on the surface of the nanoparticles. It also gives access to size-related data via DOSY NMR. For larger (plasmonic) nanoparticles, NMR spectroscopy is not applicable; therefore, much less is known in these cases about the nature of the ligand shell (see, e.g., refs. [46, 47, 49]).

The particles were not stable upon heating, although rhenium is a high-melting metal. Thermogravimetry in oxygen showed an almost complete mass loss up to 1000 °C (Fig. 8). After an initial loss of about 6 wt% up to 150 °C that can probably be assigned to adsorbed water, almost all remaining mass was lost in a sequence of barely distinguishable steps. Besides the expected combustion of the organic ligand glutathione, dirhenium heptoxide, Re_2O_7, evaporates. It has been reported that Re_2O_7

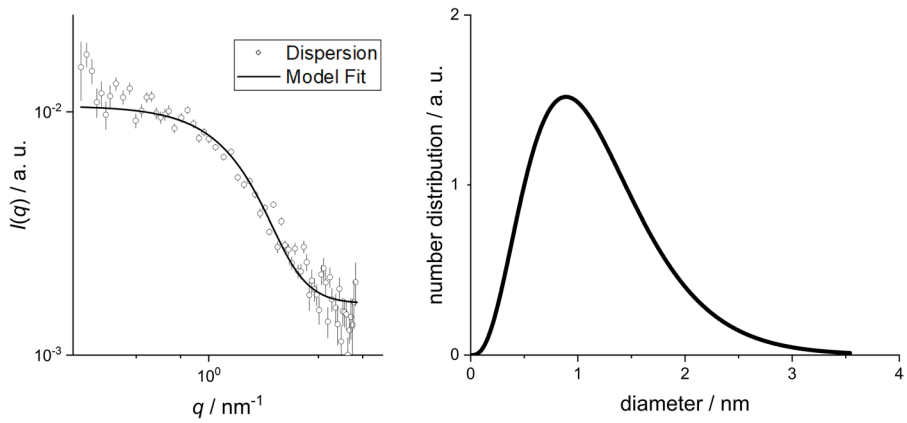

Fig. 4 Small-angle X-ray scattering (SAXS) of glutathione-coated ultrasmall rhenium nanoparticles, dispersed in water (left). Scattering data (points) and model fit (solid lines). Computed particle size distribution by number (right)

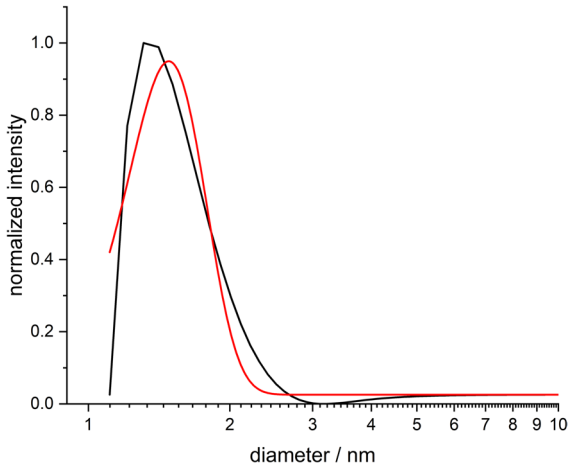

Fig. 5 Differential centrifugal sedimentation (DCS) of glutathione-coated ultrasmall rhenium nanoparticles, dispersed in water. Measured data are shown in black and a Gaussian fit curve in red

forms upon heating rhenium in air by oxidation and evaporates undecomposed at 360 °C [57]. The rapid oxidation of rhenium nanoparticles by air and water even at ambient temperature has also been frequently reported [14, 16, 24, 27].

X-ray powder diffraction on the nanoparticles heated to 300 °C in oxygen showed that the sample was almost unchanged. At further increased temperature, oxidation occurred. At 500 °C, two different rhenium oxides (ReO_2 and ReO_3) had formed, together with sodium perrhenate, $NaReO_4$. The latter has probably emerged by the presence of sodium as a counterion to deprotonated glutathione under basic synthesis conditions. At 700 °C, it was the only phase that had remained (Fig. 9). All phases formed at elevated temperature had a much larger crystallite size as indicated by the narrow diffraction peaks.

A more detailed investigation by Rietveld refinement showed that the as-prepared nanoparticles were crystalline with the hexagonal rhenium metal structure (Fig. 10). Despite the strong peak broadening that was caused by the small crystallite size, Rietveld refinement gave reliable and quantitative results. The unit cell parameters are reasonably close to those of bulk rhenium with $a = 2.7610$ Å and $c = 4.4584$ Å (ICDD #05–0702). The crystallite size was 1.5 and 1.6 nm at 25 °C and 300 °C, respectively; i.e., it was only insignificantly changed by heating to 300 °C. The comparison with the particle diameter by the other methods showed that the particles were single-crystalline, in good agreement with the TEM results (Fig. 2). This means that each nanoparticle consists of only one crystalline domain and is not twinned. Twinning has been frequently observed for nanoparticles of different sizes [58–61]. A Rietveld fit for the sample obtained at 500 °C was not possible due to the many different crystalline phases.

Table 1 summarizes all analytical data of the rhenium nanoparticles. Taken together, the particles had a high degree of uniformity and consisted of single-crystalline hexagonal metallic rhenium, still unchanged at 300 °C.

Ultrasmall rhenium nanoparticles have been prepared before, usually as heterogeneous catalysts. The

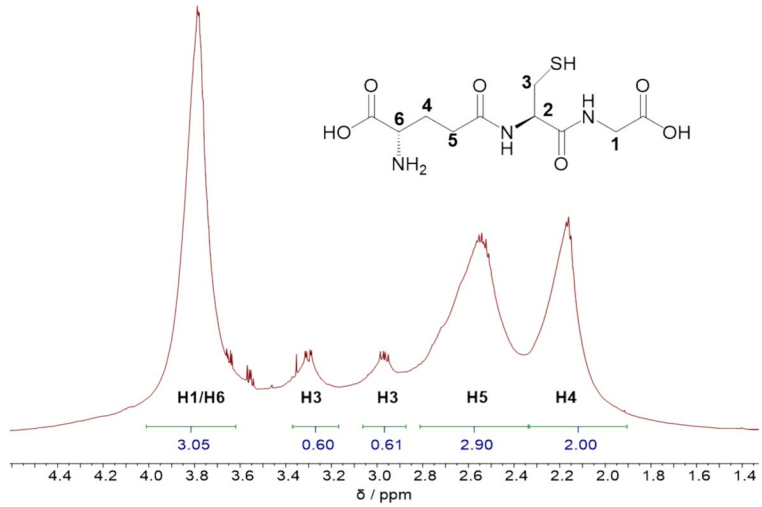

Fig. 6 ^{1}H-NMR spectrum of glutathione-coated ultrasmall rhenium nanoparticles, dispersed in 100% D_2O, and the structure of glutathione that is attached to the rhenium surface via the central cysteine thiol group. The strongly broadened NMR signals result from the vicinity of the metal core to the ligands. The integrals (blue numbers) were obtained within the green-labeled ranges

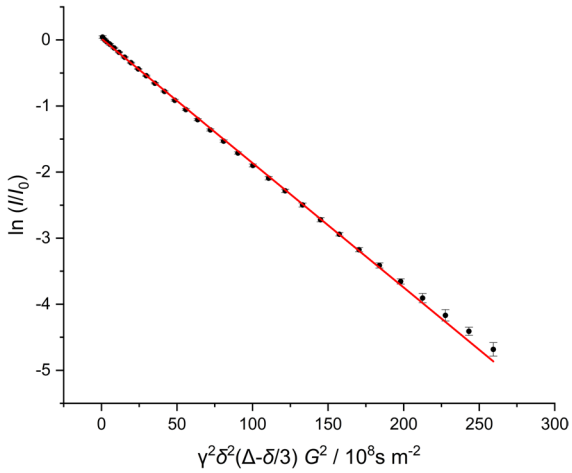

Fig. 7 Stejskal-Tanner plot from ^{1}H-DOSY NMR experiments of glutathione-coated ultrasmall rhenium nanoparticles, dispersed in 90% H_2O/10% D_2O. The data points show the average of all analyzed ^{1}H signals. The error bars show the standard deviation of the mean

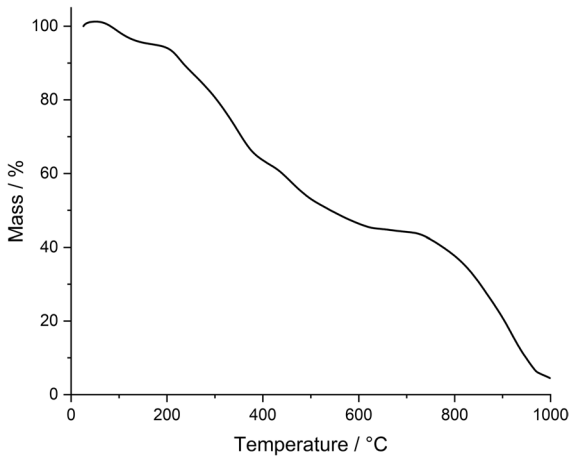

Fig. 8 Thermogravimetry of glutathione-coated ultrasmall rhenium nanoparticles in oxygen. The mass loss is due to evaporation of water, followed by combustion of the organic ligand glutathione and evaporation of rhenium heptaoxide, Re_2O_7, that forms by oxidation of rhenium with oxygen at elevated temperature and has a boiling point of 360 °C. Thus, the sample has almost completely lost its mass at 1000 °C

thermal decomposition of a dirhenium tetraallyl complex in a reducing atmosphere resulted in rhenium particles of 1 to 1.2 nm in diameter [62]. In another approach, rhenium nanoparticles were synthesized in isooctane/water mixtures by reduction of ammonium perrhenate(+VII) with natural polyphenols, leading

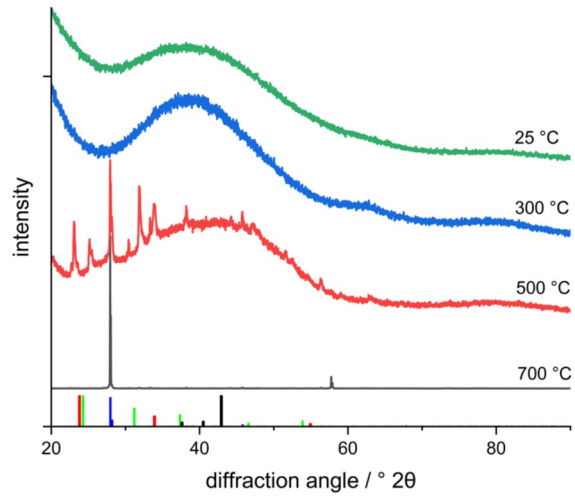

Fig. 9 X-ray powder diffractograms of glutathione-coated ultrasmall rhenium nanoparticles as-prepared (25 °C), heated to 300 °C, 500 °C, and 700 °C in oxygen in the thermobalance, respectively. At the bottom, the peak positions of elemental rhenium are shown in black (ICDD #05–0702), those of rhenium dioxide (ICDD #71–2414) in green, those of rhenium trioxide (ICDD # 72–1302) in red, and those of sodium perrhenate (ICDD #89–0326) in blue

to a broad particle size distribution between 1 and 12 nm [63]. Small rhenium nanoparticles were reported with DNA (0.7 to 1.1 nm particle size) [64], polyallylamine hydrochloride (PAH; 0.7 to 1.7 nm particle size) [65], and polyvinylpyrrolidone (PVP; 0.7 to 2.8 nm particle size) [66] as stabilizers. Shiri et al. prepared ultrasmall rhenium nanoparticles with an average diameter of 2.2 nm in a water-in-oil microemulsion. In the HRTEM, they were amorphous. Interestingly, it was found that the microemulsion surfactant dioctyl sulfosuccinate sodium (AOT) protected the rhenium nanoparticles from oxidation to perrhenate in an air atmosphere [67]. Zhong et al. prepared 6-nm rhenium nanoparticles on carbon nanotubes (CNTs) as potential catalysts by a thermal shock method (heating for about 2 s to 800 °C under argon) [12]. Preuss et al. prepared very small rhenium nanoparticles (about 1 nm diameter) by reduction with $NaBH_4$ and stabilization with polyamidoamine (PAMAM) dendrimers. XPS indicated considerable oxidation to rhenium oxides [14]. Ribeiro et al. prepared 1–4-nm rhenium nanoparticles supported on carbon and found considerable catalytic activity in

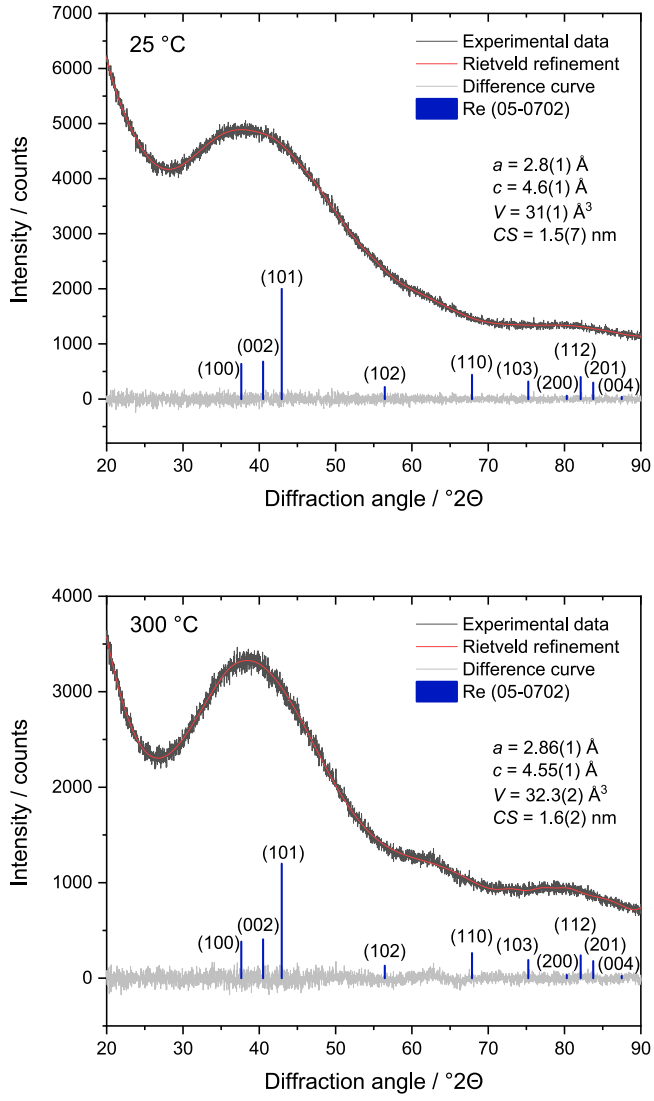

Fig. 10 Rietveld refinement of X-ray powder diffraction data of glutathione-coated ultrasmall rhenium nanoparticles as-prepared (25 °C; top, $R_{wp} = 1.83$) and after heating to 300 °C (bottom, $R_{wp} = 2.51$). Peak positions of elemental rhenium are shown in blue (ICDD #05–0702)

Table 1 Analytical data of glutathione-coated ultrasmall rhenium nanoparticles

Hydrodynamic diameter (DCS)	1.5 ± 0.3 nm
Hydrodynamic diameter (^{1}H-DOSY NMR)	2.2 ± 0.4 nm
Particle core diameter (SAXS)	1.2 ± 0.2 nm
Particle core diameter (HRTEM)	1.7 ± 0.5 nm
Crystallite size (XRD) at 25 °C	1.5 ± 0.7 nm
Crystallite size (XRD) at 300 °C	1.6 ± 0.2 nm

the reduction of 4-nitrophenol to 4-aminophenol [15]. However, the synthesis of colloidally stable and well water-dispersible metallic rhenium nanoparticles has not yet been reported.

Conclusions

It was possible to prepare ultrasmall metallic rhenium nanoparticles as monodisperse water-dispersible ultrasmall nanoparticles with an average diameter of about 1.5 nm. NMR spectroscopy confirmed the integrity of the glutathione ligand. Transmission electron microscopy and X-ray powder diffraction confirmed the presence of metallic rhenium in the

particle core. Notably, the particles were stable up to 300 °C but evaporated almost completely upon heating due to oxidation to dirhenium heptoxide that is volatile above 360 °C. This means that they are not suitable for high-temperature conversions, e.g., to obtain rhenium-based materials via powder metallurgy. Heating in the absence of oxygen will lead to the thermolysis of the organic ligand glutathione and the formation of carbides or elemental carbon. However, water-dispersible crystalline ultrasmall rhenium has a very high specific surface area and should be excellent catalysts, i.e., in dispersion or on solid supports, e.g., for electrochemical water splitting.

Acknowledgements We thank Dr. Torsten Schaller and Dr. Felix Niemeyer for carrying out the NMR experiments. M.E. and C.L.P.O. are grateful to the German Academic Exchange Service (DAAD) and Fundação Coordenação de Aperfeiçoamento de Pessoal de Nível Superior (CAPES—Finance Code 001) for generous funding of a joint project in the framework of PROBRAL/PPP. C.L.P.O. is grateful for the grant #2016/24531-3, São Paulo Research Foundation (FAPESP).

Author contribution N.K., O.P., K.L., M.H., C.L.P.O., C.B. and P.B. performed experiments and contributed to their evaluation. M.E. conceptualized and supervised the research work. All authors contributed to the manuscript. All authors reviewed the manuscript.N.K., O.P., K.L., M.H., C.L.P.O., C.B. and P.B. performed experiments and contributed to their evaluation.M.E. conceptualized and supervised the research work.All authors contributed to the manuscript.All authors reviewed the manuscript.

Funding Open Access funding enabled and organized by Projekt DEAL.

Data availability No datasets were generated or analysed during the current study.

Declarations

Competing interests The authors declare no competing interests.

References

1. Kon K, Onodera W, Toyao T, Shimizu KI (2016) Supported rhenium nanoparticle catalysts for acceptorless dehydrogenation of alcohols: structure-activity relationship and mechanistic studies. Catal Sci Technol 6:5864–5870
2. Bhama S, Sibakoti TR, Jasinski JB, Zamborini FP (2020) Highly active, selective, and recyclable water-soluble glutathione-stabilized Pd and Pd-alloy nanoparticle catalysts in biphasic solvent. ChemCatChem 12:2253–2261
3. Krajczewski J, Ambroziak R, Kudelski A (2022) Formation and selected catalytic properties of ruthenium, rhodium, osmium and iridium nanoparticles. RSC Adv 12:2123–2144
4. Watson AM, Zhang X, Alcaraz La, de Osa R, Marcos Sanz J, Gonzalez F, Moreno F et al (2015) Rhodium nanoparticles for ultraviolet plasmonics. Nano Lett 15:1095–1100
5. Linic S, Christopher P, Ingram DB (2011) Plasmonic-metal nanostructures for efficient conversion of solar to chemical energy. Nat Mater 10:911–921
6. Carter JL, McVinker GB, Weissman W, Kmak MS, Sinfelt JH (1982) Bimetallic catalysts; application in catalytic reforming. Appl Catal 3:327–346
7. Kim HD, Park HJ, Kim TW, Jeong KE, Chae HJ, Jeong SY et al (2012) The effect of support and reaction conditions on aqueous phase reforming of polyol over supported Pt–Re bimetallic catalysts. Catal Today 185:73–80
8. Kirilin AV, Tokarev AV, Manyar H, Hardacre C, Salmi T, Mikkola JP et al (2014) Aqueous phase reforming of xylitol over Pt-Re bimetallic catalyst: effect of the Re addition. Catal Today 223:97–107
9. Dobrzanska-Danikiewicz AD, Wolany W (2016) A rhenium review - from discovery to novel applications. Arch Mater Sci Eng 82:70–78
10. Chong YY, Chow WY, Fan WY (2012) Preparation of rhenium nanoparticles via pulsed-laser decomposition and catalytic studies. J Colloid Interface Sci 369:164–169
11. Karan HI, Sasaki K, Kuttiyiel K, Farberow CA, Mavrikakis M, Adzic RR (2012) Catalytic activity of platinum monolayer on iridium and rhenium alloy nanoparticles for the oxygen reduction reaction. ACS Catal 2:817–824
12. Zhong G, Zhao R, Shi YR, Li CR, He L, He L et al (2023) Thermal shock synthesis of carbon nanotubes supporting small-sized rhenium nanoparticles for efficient electrocatalytic hydrogen evolution. Rare Met 42:2166–2173
13. Ramirez AMR, Heidari S, Vergara A, Aguilera MV, Preuss P, Camarada MB et al (2023) Rhenium-based electrocatalysts for water splitting. ACS Mater Au 3:177–200
14. Preuss P, Mendez GY, Hormazabal-Campos C, Ramirez AMR, Angel FA, Camarada MB (2024) Rhenium and rhenium-copper nanoparticles: evaluation of the catalytic

activity for the decomposition of ammonium perchlorate. Catal Lett 154:1970–1981
15. Ribeiro APC, Santos BM, Faustino RFC, Pombeiro AJL, Martins LMDRS (2022) C-heterogenized Re nanoparticles as effective catalysts for the reduction of 4-nitrophenol and oxidation of 1-phenylethanol. Catalysts 12:285
16. Cyganowski P, Dzimitrowicz A (2022) Heterogenous nanocomposite catalysts with rhenium nanostructures for the catalytic reduction of 4-nitrophenol. Sci Rep 12:6228
17. Cao J, Wang Y, Yu J, Xia J, Zhang C, Yin D et al (2004) Preparation and radiolabeling of surface-modified magnetic nanoparticles with rhenium-188 for magnetic targeted radiotherapy. J Magn Magn Mater 277:165–174
18. Tu W, Denizot B (2007) Synthesis of small-sized rhenium sulfide colloidal nanoparticles. J Colloid Interface Sci 310:167–170
19. Xie CL, Niu ZQ, Kim D, Li MF, Yang PD (2020) Surface and interface control in nanoparticle catalysis. Chem Rev 120:1184–1249
20. Rodrigues TS, da Silva AGM, Camargo PHC (2019) Nanocatalysis by noble metal nanoparticles: controlled synthesis for the optimization and understanding of activities. J Mater Chem A 7:5857–5874
21. Liu LC, Corma A (2018) Metal catalysts for heterogeneous catalysis: from single atoms to nanoclusters and nanoparticles. Chem Rev 118:4981–5079
22. Schöttle C, Bockstaller P, Popescu R, Gerthsen D, Feldmann C (2015) Sodium-naphthalenide-driven synthesis of base-metal nanoparticles and follow-up reactions. Angew Chem Int Ed 54:9866–9870
23. Gyger F, Bockstaller P, Gerthsen D, Feldmann C (2013) Ammonia-in-oil-microemulsions and their application. Angew Chem Int Ed 52:12443–12447
24. Mucalo MR, Bullen CR (2001) Rhenium-based hydrosols: preparation and properties. J Colloid Interface Sci 239:71–77
25. Taratanov NA, Yurkov GY, Koksharov YA, Bouznik VM (2011) Preparation and properties of composite materials based on rhenium-containing nanoparticles and micrograins of polytetrafluoroethylene. Inorg Mater 2:118–124
26. Shiri MSZ, Henderson W, Mucalo MR (2019) A review of the lesser-studied microemulsion-based synthesis methodologies used for preparing nanoparticle systems of the noble metals, Os, Re, Ir and Rh. Materials 12:1896
27. Babu KM, Mucalo MR (2003) XPS studies of freshly prepared rhenium nanoparticle dispersions from hydrazinium hydrate and borohydride reduction of hexachlororhenate solutions. J Mater Sci Lett 22:1755–1757
28. Yang G, Wang ZP, Du FL, Jiang FY, Yuan X, Ying JY (2023) Ultrasmall coinage metal nanoclusters as promising theranostic probes for biomedical applications. J Am Chem Soc 145:11879–11898
29. Epple M, Rotello VM, Dawson K (2023) The why and how of ultrasmall nanoparticles. Acc Chem Res 56:3369–3378
30. Zheng KY, Xie JP (2020) Engineering ultrasmall metal nanoclusters as promising theranostic agents. Trends Chem 2:665–679
31. Zarschler K, Rocks L, Licciardello N, Boselli L, Polo E, Garcia KP et al (2016) Ultrasmall inorganic nanoparticles: state-of-the-art and perspectives for biomedical applications. Nanomedicine Nanotechnol Biol Med 12:1663–1701
32. Schaaff TG, Knight G, Shafigullin MN, Borkman RF, Whetten RL (1998) Isolation and selected properties of a 10.4 kDa gold:glutathione cluster compound. J Phys Chem B 102:10643–10646
33. Schaaff TG, Whetten RL (2000) Giant gold−glutathione cluster compounds: intense optical activity in metal-based transitions. J Phys Chem B 104:2630–2641
34. Heggen M, Luysberg M, Tillmann K (2016) FEI Titan 80–300 STEM. J Large-Scale Res Facil JLSRF 2:A42
35. Schneider CA, Rasband WS, Eliceiri KW (2012) NIH image to ImageJ: 25 years of image analysis. Nat Methods 9:671–675
36. Hammersley AP (2016) Fit2d: a multi-purpose data reduction, analysis and visualization program. J Appl Crystallogr 49:646–652
37. Oliveira CLP, Vorup-Jensen T, Andersen CBF, Andersen GR, Pedersen JS (2009) Discovering new features of protein complexes structures by small-angle X-ray scattering. In: Gomez M, Nogales A, Garcia-Gutierrez MC, Ezquerra TA (eds) Applications of synchrotron light to scattering and diffraction in materials and life sciences. Springer Berlin Heidelberg, Berlin, Heidelberg pp 231–244
38. Garcia PRAF, Loza K, Daumann S, Grasmik V, Pappert K, Rostek A et al (2019) Combining small-angle x-ray scattering and x-ray powder diffraction to investigate size, shape and crystallinity of silver, gold and alloyed silver-gold nanoparticles. Braz J Phys 49:183–190
39. Stejskal EO, Tanner JE (1965) Spin diffusion measurements: spin echoes in the presence of a time-dependent field gradient. J Chem Phys 42:288–292
40. Altieri AS, Hinton DP, Byrd RA (1995) Association of biomolecular systems via pulsed-field gradient NMR self-diffusion measurements. J Am Chem Soc 117:7566–7567
41. Einstein A (1905) Über die von der molekularkinetischen Theorie der Wärme geforderte Bewegung von in ruhenden Flüssigkeiten suspendierten Teilchen. Ann Phys (Berl) 322:549–560
42. Jin R, Zeng C, Zhou M, Chen Y (2016) Atomically precise colloidal metal nanoclusters and nanoparticles: fundamentals and opportunities. Chem Rev 116:10346–10413
43. Sharma S, Kim B, Lee D (2012) Water-soluble Pd nanoparticles capped with glutathione: synthesis, characterization, and magnetic properties. Langmuir 28:15958–15965
44. Creighton JA, Eadon DG (1991) Ultraviolet-visible absorption spectra of the colloidal metallic elements. J Chem Soc Faraday Trans 87:3881–3891
45. Fissan H, Ristig S, Kaminski H, Asbach C, Epple M (2014) Comparison of different characterization methods for nanoparticle dispersions before and after aerosolization. Anal Methods 6:7324–7334
46. Wolff N, Beuck C, Schaller T, Epple M (2024) Possibilities and limitations of solution-state NMR spectroscopy to analyze the ligand shell of ultrasmall metal nanoparticles. Nanoscale Adv 6:3285–3298
47. Salassa G, Burgi T (2018) NMR spectroscopy: a potent tool for studying monolayer-protected metal nanoclusters. Nanoscale Horiz 3:457–463

48. Guo C, Yarger JL (2018) Characterizing gold nanoparticles by NMR spectroscopy. Magn Reson Chem 56:1074–1082
49. Marbella LE, Millstone JE (2015) NMR techniques for noble metal nanoparticles. Chem Mater 27:2721–2739
50. Klein K, Loza K, Heggen M, Epple M (2021) An efficient method for covalent surface functionalization of ultrasmall metallic nanoparticles by surface azidation, followed by copper-catalyzed azide-alkyne cycloaddition. ChemNanoMat 7:1330–1339
51. van der Meer SB, Loza K, Wey K, Heggen M, Beuck C, Bayer P et al (2019) Click chemistry on the surface of ultrasmall gold nanoparticles (2 nm) for covalent ligand attachment followed by NMR spectroscopy. Langmuir 35:7191–7204
52. Wolff N, Prymak O, Bialas N, Schaller T, Loza K, Niemeyer F et al (2024) Conversion of ultrasmall glutathione-coated silver nanoparticles during dispersion in water into ultrasmall silver sulfide nanoparticles. Nanomaterials 14:1449
53. Wolff N, Loza K, Heggen M, Schaller T, Niemeyer F, Bayer P et al (2023) Ultrastructure and surface composition of glutathione-terminated ultrasmall silver, gold, platinum, and alloyed silver–platinum nanoparticles (2 nm). Inorg Chem 62:17470–17485
54. Wetzel O, Hosseini S, Loza K, Heggen M, Prymak O, Bayer P et al (2021) Metal–ligand interface and internal structure of ultrasmall silver nanoparticles (2 nm). J Phys Chem B 125:5645–5659
55. Biasi F, Mancin F, Rastrelli F (2020) Nanoparticle-assisted NMR spectroscopy: a chemosensing perspective. Prog Nucl Magn Reson Spectrosc 117:70–88
56. Wagner LS, Prymak O, Schaller T, Beuck C, Loza K, Niemeyer F et al (2024) The molecular footprint of peptides on the surface of ultrasmall gold nanoparticles (2 nm) is governed by steric demand. J Phys Chem B 128:4266–4281
57. Martens H, Ziegenbalg S (1973) Oxydationsuntersuchungen an Rheniumpulver: Der Re2O7-Dampfdruck. Z Anorg Allg Chem 401:145–157
58. Zhou S, Zhao M, Yang TH, Xia YN (2019) Decahedral nanocrystals of noble metals: synthesis, characterization, and applications. Mater Today 22:108–131
59. Liang C, Yu Y (2019) Understanding the formation of multiply twinned structure in decahedral intermetallic nanoparticles. IUCr J 6:447–453
60. Banerjee S, Liu CH, Lee JD, Kovyakh A, Grasmik V, Prymak O et al (2018) Improved models for metallic nanoparticle cores from atomic pair distribution function (PDF) analysis. J Phys Chem C 122:29498–29506
61. Yang H, Wang Y, Chen X, Zhao X, Gu L, Huang H et al (2016) Plasmonic twinned silver nanoparticles with molecular precision. Nat Commun 7:12809
62. Ayvali T, Lecante P, Fazzini PF, Gillet A, Philippot K, Chaudret B (2014) Facile synthesis of ultra-small rhenium nanoparticles. Chem Commun 50:10809
63. Revina AA, Kuznetsov MA, Chekmarev AM (2013) Physicochemical properties of rhenium nanoparticles obtained in reverse micelles. Dokl Chem 450:119–121
64. Anantharaj S, Sakthikumar K, Elangovan A, Ravi G, Karthik T, Kundu S (2016) Ultra-small rhenium nanoparticles immobilized on DNA scaffolds: an excellent material for surface enhanced raman scattering and catalysis studies. J Colloid Interface Sci 483:360–373
65. Kundu S, Ma L, Dai W, Chen Y, Sinyukov AM, Liang H (2017) Polymer encapsulated self-assemblies of ultrasmall rhenium nanoparticles: catalysis and SERS applications. ACS Sustain Chem Eng 5:10186–10198
66. Bedia J, Calvo L, Lemus J, Quintanilla A, Casas JA, Mohedano AF et al (2015) Colloidal and microemulsion synthesis of rhenium nanoparticles in aqueous medium. Colloids Surf A Physicochem Eng Asp 469:202–210
67. Shiri MSZ, Henderson W, Henning AM, Mucalo MR (2024) Synthesis study of size-controlled rhenium nanoparticle systems using reverse micelle-based methodologies. Coll Surf A 694:134150